Received: 11 March 2024 | Revised: 15 June 2024 | Accepted: 20 June 2024

DOI: 10.1002/mrm.30211

RESEARCH ARTICLE

Magnetic Resonance in Medicine

Acoustic noise reduction in the NexGen 7 T scanner

Nicolas Boulant[1,2,3] | **Samantha Ma**[4] | **Erica Walker**[2,3] | **Alexander Beckett**[2,3] | **An T. Vu**[5,6] | **Shajan Gunamony**[7] | **David A. Feinberg**[2,3]

[1]CEA, CNRS, BAOBAB, NeuroSpin, University of Paris-Saclay, Gif sur Yvette, France

[2]Brain Imaging Center, Helen Wills Neuroscience Institute, University of California, Berkeley, California, USA

[3]Advanced MRI technologies, Sebastopol, California, USA

[4]Siemens Healthcare, Malvern, Pennsylvania, USA

[5]University of California, San Francisco, California, USA

[6]San Francisco VA Health Care System, San Francisco, California, USA

[7]Imaging Centre of Excellence, University of Glasgow, Glasgow, United Kingdom

Correspondence
David A. Feinberg, Brain Imaging Center, Helen Wills Neuroscience Institute, Department of Neuroscience, University of California, Berkeley, CA, USA.
Email: david.feinberg@berkeley.edu

Funding information
European Union, Grant/Award Number: 885876; >National Institutes of Health, Grant/Award Numbers: R44-MH129278, U01-EB025162, U24-NS129949

Abstract

Purpose: Driven by the Lorentz force, acoustic noise may arguably be the next physiological challenge associated with ultra-high field MRI scanners and powerful gradient coils. This work consisted of isolating and mitigating the main sound pathway in the NexGen 7 T scanner equipped with the investigational Impulse head gradient coil.

Methods: Sound pressure level (SPL) measurements were performed with and without the RF coil to assess its acoustic impact. Vibration measurements were carried out on the gradient coil, the RF coil, and on the patient table to distinguish the different vibration mechanisms and pathways. Vibrations of the RF coil were modified by either making contact with the patient bore liner with padding material or by changing directly the RF shield with phosphor bronze mesh material.

Results: SPL and vibration measurements demonstrated that eddy-currents induced in the RF shield were the primary cause of acoustic noise. Replacing the conventional solid copper shield with phosphor bronze mesh material altered the vibrations of the RF shield and decreased SPL by 6 to 8 dB at the highest frequencies in EPI, depending on the gradient axis, while boosting the transmit B_1^+ field by 15%. Padding led to slightly less sound reduction on the X and Z gradient axes, but with minimal impact for the Y axis.

Conclusion: This study demonstrates the potential importance of eddy-current induced vibrations in the RF coil in terms of acoustic noise and opens new horizons for mitigation measures.

KEYWORD
acoustic noise eddy-currents RF shield vibrations

1 | INTRODUCTION

The quest for higher spatio-temporal resolutions in MRI has been a driving force for the development of more powerful magnets[1,2] and gradient coils.[3–5] After major engineering efforts and achievements, one fundamental obstacle remains physiological. In this context, the ability to reduce peripheral nerve stimulation (PNS) using head-only gradient coils without covering the thorax and

heart pushes further the limits of MR capabilities.[5] Acoustic noise yet remains inevitable and is driven by vibrations induced by the Lorentz force (i.e. the product of current times the main magnetic field B_0). Despite encouraging results regarding vibrations or sound pressure levels (SPLs) versus field strength,[1,6] fdue to increased dampening effects[7] or other gradient-magnet interactions,[8] acoustic noise in general increases with gradient strength and slew rate as well as magnetic field strengths and requires hearing protection combined with careful engineering at the design stage to remain under the regulatory limits. Modeling based on finite elements or statistical energy analysis tools[9,10] can aid scanner design, but can also be difficult given the multi-physical aspects of the problem involving vibrations, acoustics, and electromagnetism. Practical mitigation measures, besides the usual hearing protection, include foam rings around the patient bore liner for sound attenuation, active noise control,[11,12] mechanical isolation or decoupling,[13] sequence adjustments,[14–16] and special gradient inserts.[17] Strong acoustic noise levels can interfere with the stimulation paradigm of an fMRI experiment, lead to subject's discomfort or, in the worst case, to hearing loss.[18] In Feinberg et al.,[5] levels of 131 dBA were reported when running an EPI sequence at an echo-spacing (ES) of 0.56 ms. With the 33 dB attenuation commonly provided by earplugs, users now graze the 99 dBA regulatory threshold[19] and can push the ES no further without mitigating the acoustic noise.

Acoustic noise in MRI is often believed to originate mostly from the vibrations of the gradient coil.[11,20] The strong switching of currents within the gradient tube are immersed in a magnetic field and undergo Lorentz forces that grow linearly with field and current.[8] When hitting the mechanical resonances of the gradient tube, larger displacements and accelerations occur generating stronger sound pressure waves. Sound from the gradient vibration can then propagate toward the patient's ear by different transmission pathways[10] such as via air to the patient bore liner and the RF coil, which can radiate sound, or via mechanical transmission to the cryostat, patient bore liner, table, and RF coil, themselves emitting sound. Although identified in Edelstein et al.,[10] the influence of vibrations induced by the oscillating eddy-currents in the cryostat and in the shield of the RF coil are often overlooked.[6,11] Perception of sound is logarithmic, as measured in dB, making it crucial to isolate the dominating source to reduce the sound level, otherwise secondary noise contributions are masked.[10]

This work reports the investigation and mitigation of the primary acoustic noise pathway in the NexGen 7 T scanner equipped with the investigational Impulse gradient coil developed by Siemens Healthineers (Siemens Healthcare). The study is largely driven by acoustic and vibration measurements that ultimately converge toward eddy-current–induced vibrations in the shield of the RF coil. Based on these observations, two different methods to reduce them were investigated. The first method is mechanical and consists of coupling the fiberglass former of the RF coil with the patient bore liner to attempt constraining its vibrations. The second method is electromagnetic and aims at reducing directly the eddy-currents in the shield of the RF coil, thereby minimizing its vibrations, while maintaining good RF shielding properties.

2 | METHODS

Measurements were performed on the NexGen 7 T Terra scanner with the investigational Siemens Impulse head gradient coil (maximum gradient strength and slew rate of 200 mT/m and 900 mT/m/ms, respectively). Other characteristics for the gradient coil include: weight = 1060 kg, length = 1.19 m, inner diameter = 44 cm, outer diameter = 81 cm, inductance = 315/383/315 (X/Y/Z) μH and DC resistance = 55/59/48 (X/Y/Z) mΩ.[5] Vibration measurements were performed with five mono-axial accelerometers (4507-C) connected to a dedicated front-end and software (Bruël and Kjaer). Gradient frequency sweeps were performed with chirp pulses separately for each gradient axis for 2 min over the 0 to 3.2 kHz interval and at 5 mT/m. Accelerations were measured in real-time and transfer function spectra were computed with Fourier analysis. SPL measurements were performed either at fixed EPI ES or frequencies using an optical probe (Optoacoustics) or with a condenser 4188–1-021 microphone (Bruël and Kjaer), depending on the availability of the equipment, for the same frequency sweeps as for the vibrations and combined with Fourier analysis. During a ramp down of the magnet, a gradient sweep along each axis was performed at 0 T (i.e., with no vibrations) with the microphone to verify negligible signal leakage because of the electromagnetic field generated by the currents running through the gradient coil. Background acoustic noise (mostly from the cold heads) was recorded at ~70 dB for frequencies smaller than 200 Hz. Above this frequency, background sound levels were ~40 dB. The acoustic probe was taped at the ear locations of an anthropomorphic phantom (weight = 8 kg) (Figure 1A).[21]

2.1 | Isolating the primary noise pathway

Given some preliminary measurements, and consistently with Edelstein et al.,[10] the SPL was measured with and without the main RF coil used in the lab. It is an 8Tx-64Rx RF coil (MR CoilTech) whose specifications can be found

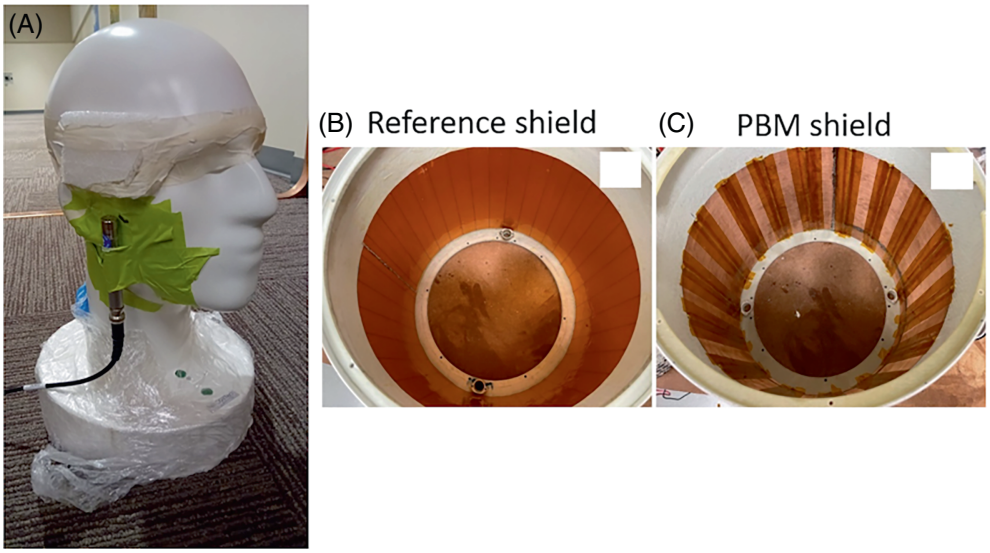

FIGURE 1 Experimental setup. (A) Acoustic noise microphone sensor attached to the right ear of an anthropomorphic head phantom. (B) Photograph of the reference double layered RF shield realized using flexible PCB. There are a total of 34 longitudinal strips of width 32 mm each. (C) Photograph of the phosphor bronze mesh (PBM) shield with 16 strips. The adjacent strips are bridged with 1000 pF capacitors.

in Feinberg et al.[5] The reference RF shield was a conventional two-layered design consisting of 34 longitudinal strips in each layer with a strip width of 32 mm and copper thickness of 18 μm (Figure 1B). After establishing the importance of the presence of the RF coil in generating the acoustic noise, further measurements targeted the identification of the main sound transmission pathway: mechanical transmission from the gradient coil to the patient table and RF coil or vibrations induced by eddy-currents in the shield of the RF coil. Vibration measurements on the gradient coil (for the three gradient axes, accelerations measured along the X and Y directions on the back flange), on the RF coil, and on the patient table were performed to visualize potential similarities with the SPL spectra. To discriminate between the two scenarios and isolate the most likely sound pathway, mechanical coupling between the RF coil and the table was modified using either a soft foam pad (used by default in the laboratory), with Sylodyn (Getzner) pads of medium softness and hard wooden wedges. Invariance of the vibration results between these three different conditions would suggest that mechanical coupling is not responsible for the acoustic noise, but that vibrations induced in the RF coil by eddy-currents would most likely be the primary cause.

2.2 | Mitigating the acoustic noise problem

After confirming that the primary pathway of acoustic noise originates from eddy-current induced vibrations of the RF coil, two mitigation strategies were investigated. First, sponge seal materials (M-D Building Products) were taped around the circumference of the fiberglass RF coil to contact with the patient bore liner (inner diameter of 39 cm) and constrain its vibrations. SPL measurements were then performed at both ear locations on an adult volunteer (male, 82 kg) who provided informed consent, with and without the padding material. The measurements were carried out with EPI sequences with ES at 0.56, 0.61, 0.66, 0.71, 0.76, 0.81, 0.96, and 1.01 ms on all gradient axes separately with an amplitude of 86 mT/m to match the high-resolution fMRI scans in Feinberg et al.[5] The 0.81 to 0.96 ms interval was skipped following Siemens instructions because of mechanical resonances that could damage the gradient coil.

The second strategy consisted of reducing vibrations of the RF shield by changing its material. For that purpose, we tried the phosphor bronze mesh (PBM) material. It was reported in Lee et al.[22] that such material could possess valuable properties that reduce eddy-currents while protecting electronic equipment in PET-MRI. Its shielding properties were also investigated in Weyers et al.[23] The PBM shield, therefore, consisted of 380 mesh count per inch (Shandong Xingying Technology) and was segmented into 16 longitudinal strips with a 2 mm gap. The adjacent strips were bridged together with 1000 pF capacitors to make the shield continuous for the RF field (see Figure 1C). The SPL spectra were measured on the head phantom with the reference and the PBM shields with segmentation. They were complemented with EPI measurements for further confirmation and to provide effective SPLs for useful MR sequences. The sound measurements with EPI pulse sequences were first performed with no segmentation (slits) on the PBM shield. To verify that reduction of acoustic noise with the PBM shield with segmentation was not at the detriment of the B_1^+ field efficiency, individual transmit field maps were measured on a 15.6 cm diameter spherical agar saline gel phantom using a turbo-FLASH sequence at 5 mm resolution and

the circular polarization (CP) mode was reconstructed. Unless specified explicitly, all experimental results with PBM presented in the manuscript (SPL, B_1^+ field) are with segmentation of the shield (16 longitudinal strips bridged by capacitors).

3 | RESULTS

Figure 2 reports the SPL measurements with and without the 8Tx-64Rx RF coil with initial solid copper shield (top row). The bottom row shows for the three gradient axes the vibration spectra measured on the gradient coil in relation to the SPL, both in linear scale. Although some peaks sometimes coincide (e.g., at 1900 Hz on the Y axis) the correspondence between the two is poor. One can see also a trend of acoustic noise level growing with frequency in the presence of the RF coil, which is not consistent with the acceleration spectrum of the gradient coil, but consistent with eddy-currents (Faraday's law).[22]

Figure 3 reports the accelerations measured for the three gradient axes and five accelerometers located on the RF coil with the solid shield. Here, the vibrations of the RF coil show more similarities with the SPL spectra of Figure 2 (bottom row) with higher amplitude trend versus frequency.

Figure 4 shows the vibration results of the patient table, with and without the RF coil, together with a

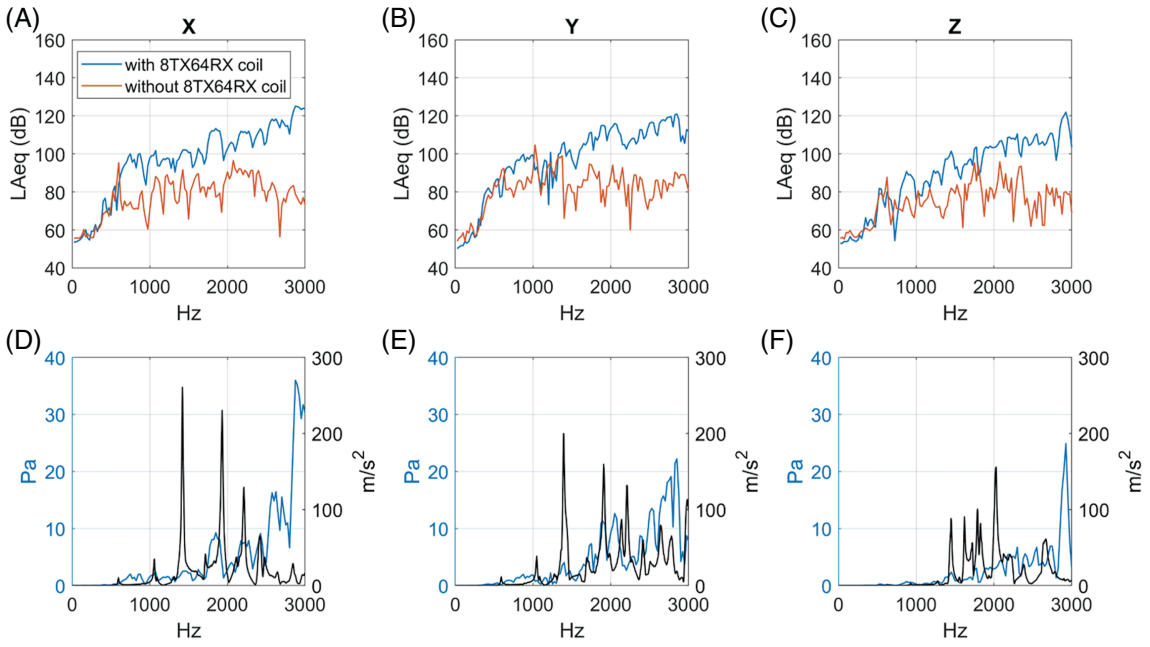

FIGURE 2 Continuous wave sound pressure level measurements at 5 mT/m with and without the RF coil. Sound pressure levels (SPLs) are shown for the three axes versus frequency (A–C) in log scale (20 μPa reference) (same color coding). The SPL with the RF coil is displayed again in (D–F) in linear scale and is aligned with measured acceleration spectra of the gradient coil (G = 1 mT/m), showing poor correspondence.

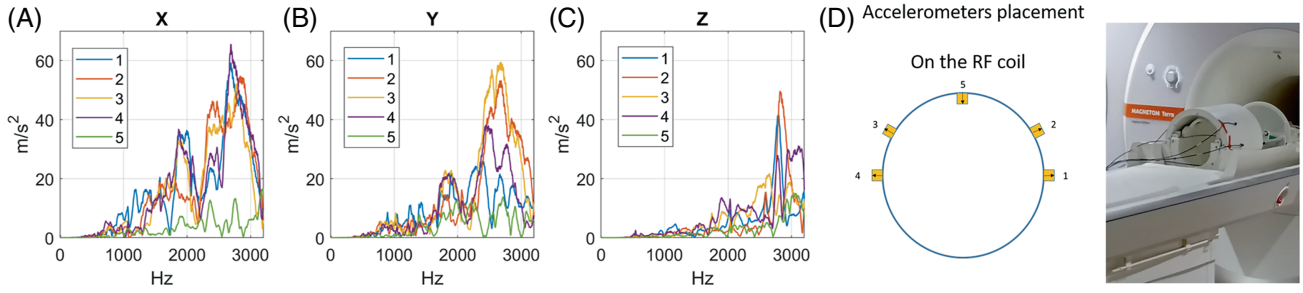

FIGURE 3 RF coil vibration measurements for G = 5 mT/m. The acceleration spectra are shown in (A–C) for the three gradient axes respectively along with a drawing and picture showing the placement of the accelerometers. The sensors are labeled 1–5 and correspond to the placement shown in (D).

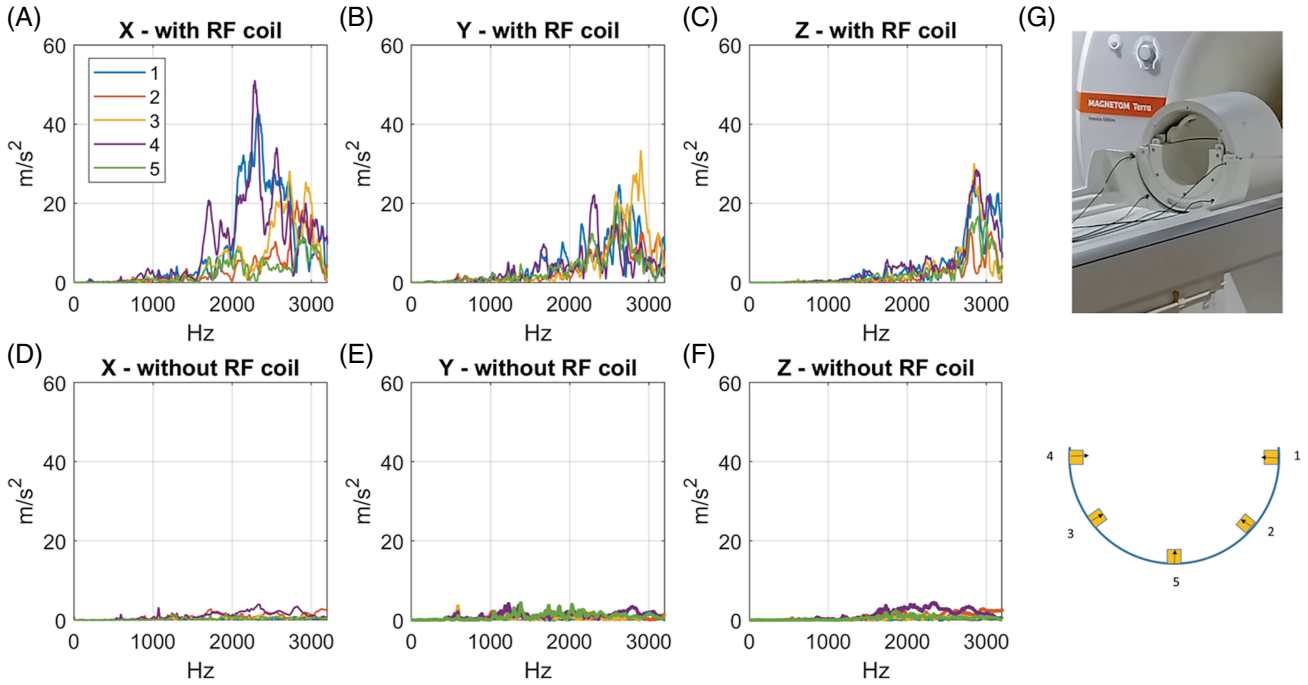

FIGURE 4 Table vibration measurements with and without the RF coil. The acceleration spectra are shown in linear scale at gradient strength of 5 mT/m in (A–C) for the three gradient axes, respectively, with the RF coil and (D–F) without. The sensors are labeled 1–5 with their respective placements shown in (G).

photograph illustrating accelerometer placement. The spectra with versus without the RF coil are plotted on the same scale to highlight the differences. In the absence of the RF coil, the patient table vibrates much less. Yet, this still does not completely prove that the table does not drive the motion of the RF coil by mechanical coupling, a small oscillating force being able to generate large vibrations through resonance. With the RF coil, the vibration spectra of the patient table again show some similarities with the ones acquired on the RF coil (Figure 3).

Figure 5 shows the RF coil vibration measurement results for the five sensors located on the RF coil with the solid shield (placement shown in Figure 3D) when sweeping along the X gradient axis at 5 mT/m for the three support materials tested: gray soft foam pad, green Sylodyn pads, and wooden wedges (shown in Figure 5F). The vibration spectra barely changed with the configurations, suggesting that the mechanical coupling between the table and the RF coil was not the leading factor for most of the RF coil vibrations. One exception was observed for sensor 3. It was later found that the sensor in these experiments could make contact with the patient bore liner, depending on the material thickness. These data led to the idea of altering RF coil vibrations using padding materials to establish contact with the bore liner.

Following this observation, strips of sponge material were placed on the outside of the RF coil fiberglass former. The thickness was varied iteratively until reasonably firm contact with the patient bore liner could be established. A picture of the setup is shown in Figure 6 together with the SPL measurements for EPI sequences at different ES. Despite a few ES where the SPL was worse with the padding (by 2 dB at the most, e.g., Y axis, right ear, ES = 0.96 ms), there was a consistent sound level reduction with the sponge materials at both ear locations, especially for the X and Z axes, reaching up to 10 dB at the shortest ES of 0.56 ms. The effect appears smaller at longer ES (i.e., lower frequencies), which is consistent with eddy-currents decreasing with decreasing frequency, thereby allowing the contribution of other acoustic noise sources.

Figure 7 reports the acoustic noise spectra measured with the head phantom with frequency sweeps on the three different gradient axes at amplitude of 5 mT/m with no RF coil, with the RF coil but no RF shield, the modified shield made of segmented PBM material, and with the reference solid RF shield. The results illustrate the improvements made with the PBM shield compared to the solid shield configuration. Interestingly, the sound levels with the PBM shield in fact are comparable to the no shield configuration, but still higher than with no RF coil at all, indicating potential remaining vibrations of other elements inside the RF coil structure or acoustic resonances induced by the RF coil.

These data are consistent with further EPI measurements showing substantial sound reduction of SPL with

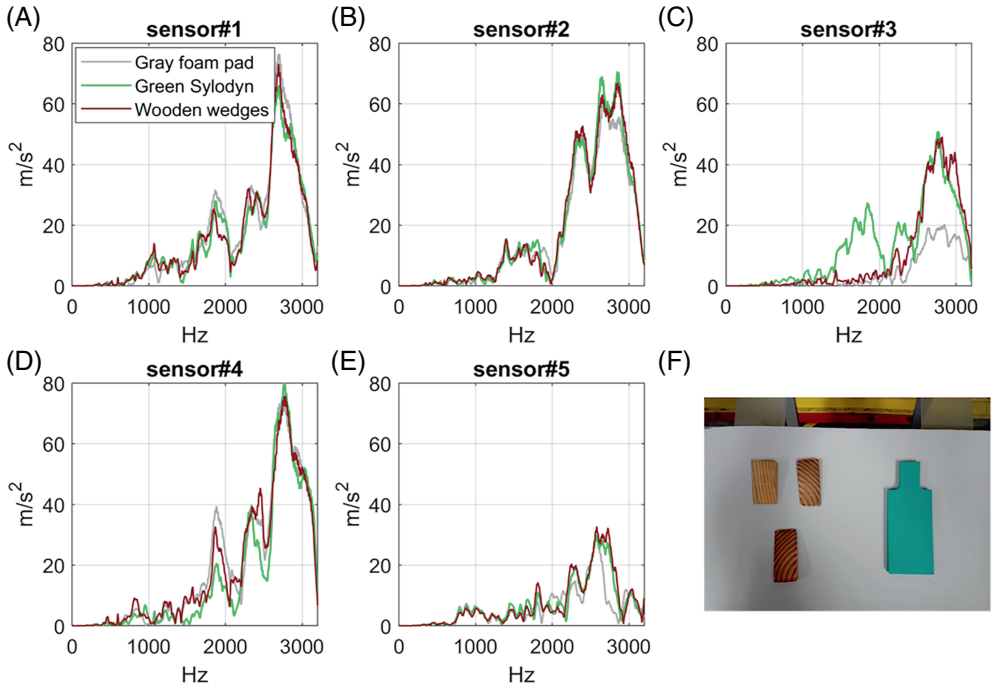

FIGURE 5 RF coil vibration measurements with different support materials. The sensors are labeled 1–5 and correspond to subplots (A–E), whereas the support materials are shown in (F).

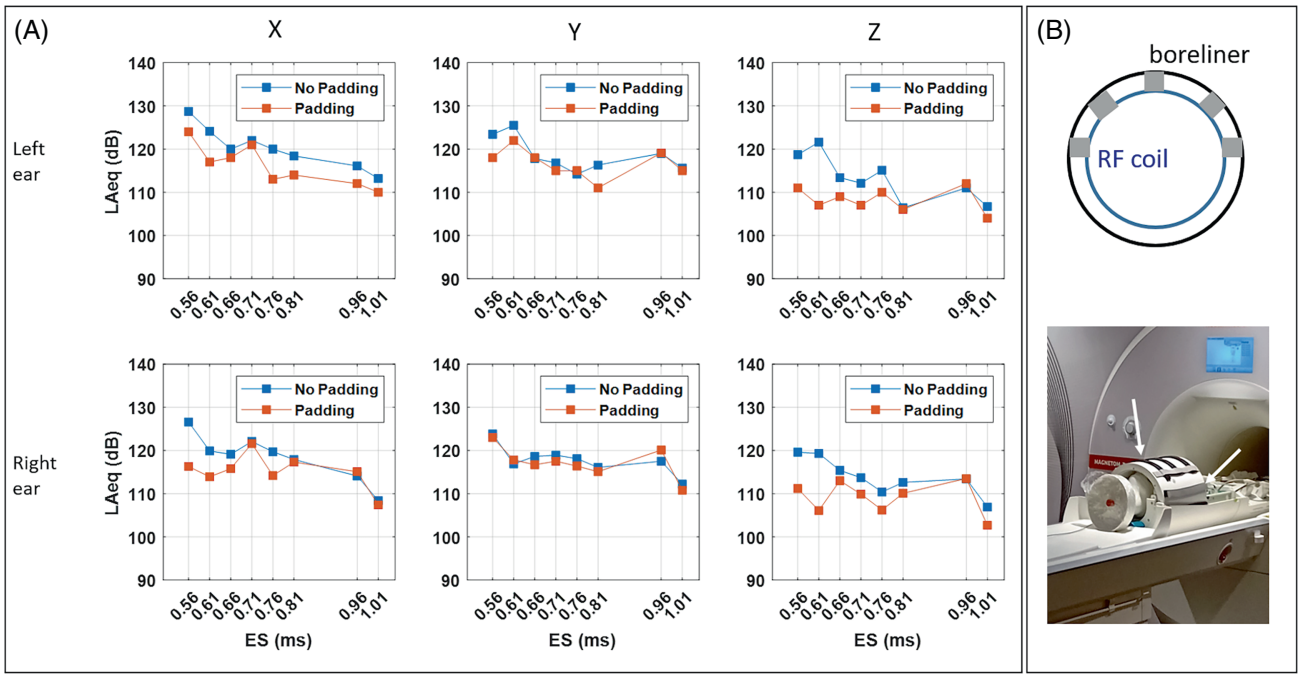

FIGURE 6 Sound pressure levels (SPLs) obtained in vivo with the padding approach and RF coil with solid copper shield. The SPLs are shown for the three different gradient axes (left to right) for the left (top) and right (bottom) ear locations in (A). The setup is illustrated in (B). The 0.56, 0.61, 0.66, 0.71, 0.76, 0.81, 0.96, and 1.01 ms echo-spacings (ES) correspond respectively to 893 (2679), 820 (2459), 758 (2273), 704 (2113), 658 (1974), 617 (1852), 521 (1563), and 495 (1485) Hz for the main (third harmonic) frequency of the EPI echo train.

the RF shield made of PBM, reaching up to 9 dB (Figure 8). One data point remains (i.e., on the Y axis at ES = 0.61 ms at the right ear location) where the PBM made it worse. The gain was otherwise systematic. Table 1 summarizes the gains made with the PBM shield for different ES. Sound level measurements for EPI with PBM, but with no segmentation (no slits) revealed worse performance (Figure S1 in Supporting Information) than for the standard shield, indicating still the importance of this feature.

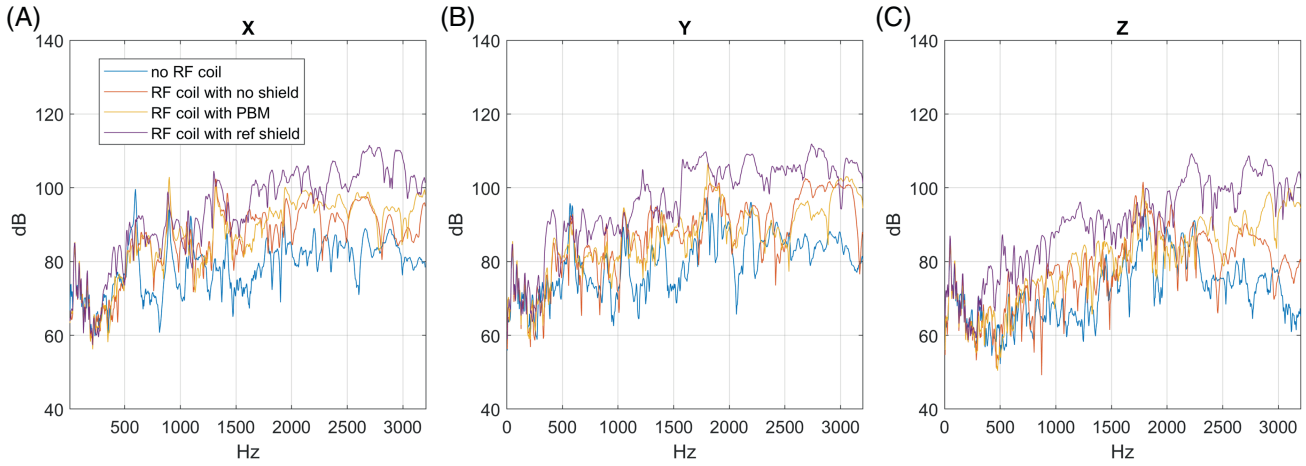

FIGURE 7 Sound pressure level spectra measured on an anthropomorphic phantom (average of responses at right and left ear locations) for the three gradient coil axes. Measurements are shown for G = 5mT/m (R1.13) and for the following configurations: no RF coil, RF coil with no shield, RF coil with segmented phosphor bronze mesh (PBM) shield, and RF coil with conventional solid shield.

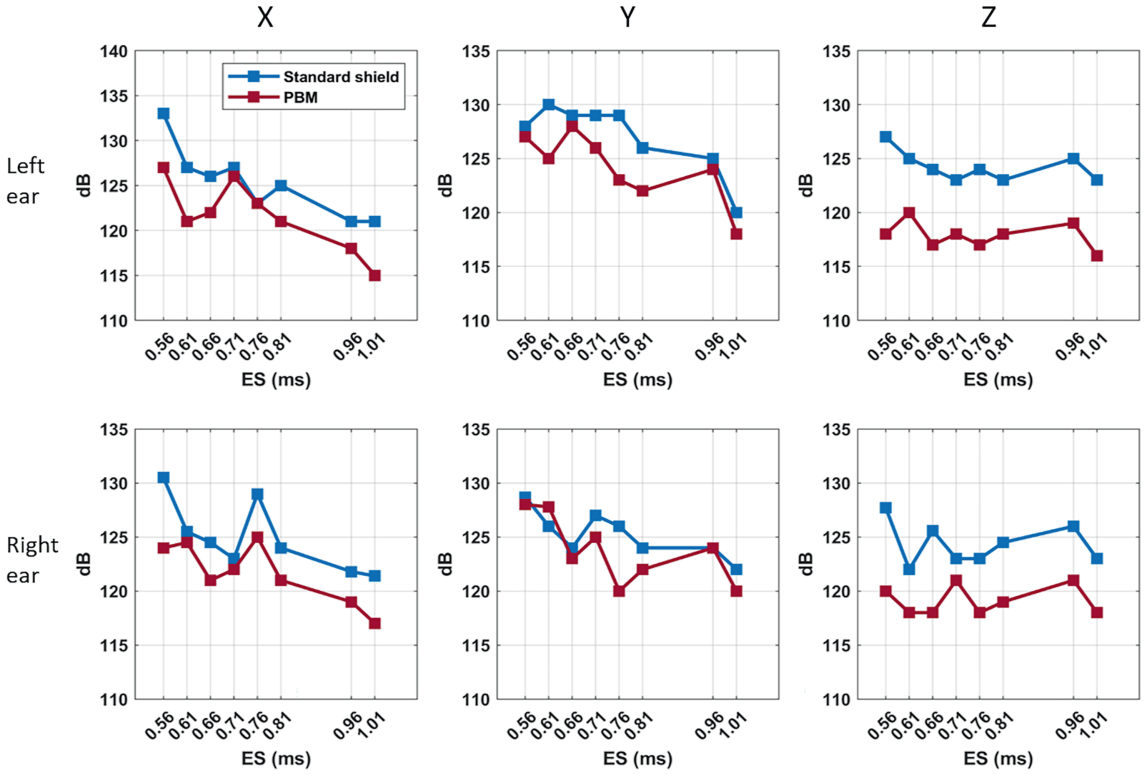

FIGURE 8 Sound pressure levels (SPLs) measured at the two ear locations of an anthropomorphic head phantom for EPI versus echo-spacings (ES), for the standard shield versus the segmented phosphor bronze mesh (PBM) shield. The SPLs are shown for the three different gradient axes (left to right) for the left (top) and right (bottom) ear locations. The 0.56, 0.61, 0.66, 0.71, 0.76, 0.81, 0.96, and 1.01 ms ES correspond respectively to 893 (2679), 820 (2459), 758 (2273), 704 (2113), 658 (1974), 617 (1852), 521 (1563), and 495 (1485) Hz for the main (third harmonic) frequency of the EPI train.

Finally, Figure 9 reports the CP mode reconstructed from the B_1^+ field map measurements, showing an increase in transmit field efficiency of 15% when using the PBM versus the reference shield.

4 | DISCUSSION

To enhance the B_1^+ field while reducing eddy-currents, the RF shield must be quasi-continuous for RF fields

TABLE 1 Acoustic noise reduction with PBM versus solid copper shield.

Axis\ES (ms)	0.56	0.61	0.66	0.71	0.76	0.81	0.96	1.01
X	6.25	3.5	3.75	1	2	3.5	2.9	5.2
Y	0.85	1.6	1	2.5	6	3	0.5	2
Z	8.35	4.5	7.3	3.5	6	5.25	5.5	6

Note: Results are provided in dB for EPI versus ES for the different gradient axes. Results were calculated as the average of the values at the left and right ear locations on the anthropomorphic phantom. A positive value represents a SPL reduction when using the PBM shield (still with segmentation) versus the solid copper shield.
Abbreviations: ES, echo spacing; PBM, phosphor bronze mesh; SPL, sound pressure level.

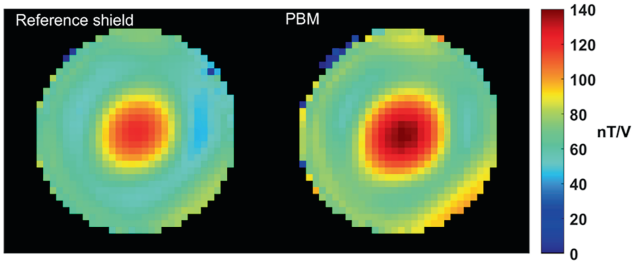

FIGURE 9 B_1^+ map field distributions in CP mode (axial view) on a spherical agar gel phantom. Left: reference solid shield. Right: segmented phosphor bronze mesh (PBM). Volts here are defined per transmit channel.

and discontinuous at kHz frequencies to disturb the eddy-currents induced by gradient activity.[23] A continuous solid copper sheet has attractive properties for the former, but must, therefore, include slits to reduce eddy current loops.[22,23] Adjacent strips are then connected with capacitors to re-establish continuity at RF frequencies. Reducing the eddy-currents with the PBM material[22] led to less vibrations in the RF coil and, therefore, SPL. In our setup, the nature of the PBM allowed reducing the number of slits compared to the reference solid copper shield and thereby increased the shielding performance, which could be confirmed by an increased transmit field efficiency of 15%. Figure S1 indicates that slits remained necessary for more acoustic performance. Given the improvements shown in Figure 7 with the PBM shield in terms of acoustic noise and the fact that the results with the PBM shield are somewhat similar to when there is no RF shield at all, it is not clear if much more acoustic performance could be obtained with further shield modifications, although stainless steel could be another material candidate.[23] However, given the remaining acoustic gap with the no RF coil scenario, there is still room for improvement considering other components in the RF coil possibly vibrating and/or acoustic resonances induced by the coil geometry. These measurements establish that, in addition to the RF shield, the structure of the RF coil itself plays a role in increasing the acoustic noise. It is important to note that the 8Tx-64Rx RF coil used in this study has a sliding mechanism to easily position the subject in the coil. This means that the coil structure incorporated two movable assemblies—the anterior half of the receive array and the transmit array. In such designs, only the front and rear end of the coil structure are mechanically coupled to the patient table, whereas in RF coils without the sliding mechanism, the entire coil body can be one single piece and is sitting on the patient table, allowing possibly fewer degrees of freedom to vibrate.

As motivated here, padding on the RF coil could be combined with the PBM material to further attenuate sound. This was not attempted because a more long-term and elegant solution was sought, given the sponge seals partially wore off each time the RF coil was moved in the scanner. With the woven nature of the PBM material taken together with the slit arrangement in our final setup, SPL measurements revealed a substantial drop by up to 8 dB at some EPI ES (Table 1). This is due mostly to the reduction of the high frequency sound response (Figure 7) in concert with a reduction of eddy-currents in the shield of the RF coil. At lower frequencies, other sound transmission pathways may dominate and the modifications of the shield in our case may not make any difference. Gradient amplitude and slew rate limits, recruitment of axes and their respective spectra and duty-cycles are unique to different MRI sequences. Therefore, it is difficult to draw general conclusions with respect to regulatory acoustic limits based on the acoustic transfer function alone (Figure 7). Therefore, it remains advised to perform net acoustic measurements for every RF coil and protocol to ensure it meets regulatory standards.

Given the interplay between magnet design, gradient coil mechanical resonance modes, the gradient stray field, and the RF coil, it would be premature to extrapolate our results to other setups. Yet, eddy-current induced noise in the inner bore of the cryostat and in an RF body coil were found to be some of the main acoustic noise sources in a 1.5 T GE scanner.[10] For a similar scanner design, the relative dominance of different noise sources in any case should not depend on the B_0 field as they should all scale similarly (Lorentz forces). In head-only scanners,

with easy access to the RF head coil, users should perform SPL measurements with and without its presence to confirm its impact and possibly investigate similar mitigation measures.

5 | CONCLUSION

We identified with SPL and vibration measurements the primary pathway of acoustic noise in the NexGen 7 T scanner that incorporates a high performance head gradient coil. After determining the impact of eddy-current induced vibrations in the shield of the RF coil, we altered its vibrations either by introducing padding material or by modifying the shield of the RF coil, reducing acoustic noise by up to 10 dB. The results pave the way for future improvements to further push MR investigations at higher field and with more powerful gradient coils.

ACKNOWLEDGMENTS

This project has received funding from National Institutes of Health (U01-EB025162, U24-NS129949, and R44-MH129278. N.B. has received funding from the European Union's Horizon 2020 research and innovation program under grant agreement no. 885876 (AROMA).

CONFLICT OF INTEREST STATEMENT

S.M. is an employee of Siemens Healthcare. S.G. is a shareholder of MR CoilTech, Glasgow, United Kingdom. D.F., E.W., N.B., and A.B. are employees of Advanced MRI Technologies.

ORCID

Nicolas Boulant https://orcid.org/0000-0003-2144-2484
Shajan Gunamony https://orcid.org/0000-0002-3146-6079

REFERENCES

1. Boulant N, Quettier L, the Iseult Consortium, et al. Commissioning of the Iseult CEA 11.7 T whole-body MRI: current status, gradient–magnet interaction tests and first imaging experience. *Magn Reson Mater Phys Biol Med*. 2023;36:175-189. doi:10.1007/s10334-023-01063-5
2. He X, Erturk MA, Grant A, et al. First in-vivo human imaging at 10.5T: imaging the body at 447 MHz. *Magn Reson Med*. 2020;84:289-303.
3. Schmitt F, Nowak S, Eberlein E. An attempt to reconstruct the history of gradient-system technology at Siemens. MAGNETOM Flash (77) 2/2020. http://clinical-mri.com/wp-content/uploads/2020/09/Schmitt_Gradient_Development_ISMRM_2020.pdf
4. Foo TKF, Ek TT, Vermilyea ME, et al. Highly efficient head-only magnetic field insert gradient coil for achieving simultaneous high gradient amplitude and slew rate at 3.0T (MAGNUS) for brain microstructure imaging. *Magn Reson Med*. 2020;83:2356-2369.
5. Feinberg DA, Beckett AJS, Vu AT, et al. Next-generation MRI scanner designed for ultra-high-resolution human brain imaging at 7 tesla. *Nat Methods*. 2023;20:2048-2057. doi:10.1038/s41592-023-02068-7
6. Moelker A, Wielopolski PA, Pattynama PMT. Relationship between magnetic field strength and magnetic resonance-related acoustic noise. *Magn Reson Mater Phys Biol*. 2003;16:52-55.
7. Winkler SA, Schmitt F, Landes H, et al. Gradient and shim technologies for ultra-high field MRI. *Neuroimage*. 2018;168:59-70.
8. Boulant N, Le Ster C, Amadon A, et al. The possible influence of third order shim coils on gradient-magnet interactions: an inter-field and inter-site study. *Magn Reson Mater Phys Biol Med*. 2023;37:169-183. doi:10.1007/s10334-023-01138-3
9. Winkler SA, Alejski A, Wade T, McKenzie CA, Rutt BK. On the accurate analysis of vibroacoustics in head insert gradient coils. *Magn Reson Med*. 2017;78:1635-1645.
10. Edelstein WA, Hedeen RA, Mallozzi RP, El-Hamamsy S-A, Ackermann RA, Havens TJ. Making MRI Quieter. *Magn Reson Imaging*. 2002;20:155-163.
11. McJury MJ. Acoustic noise and magnetic resonance imaging: a narrative/descriptive review. *J Magn Reson Imaging*. 2022;55:337-346.
12. Goldman AM, Gossman WE, Friedlander PC. Reduction of sound levels with antinoise in MR imaging. *Radiology*. 1989;173:549-550.
13. Dumoulin CL, Giaquinto R, Loew W. Acoustic noise reducing RF coil for magnetic resonance imaging. US Patent 2015/0102813 A1.
14. Osterle C, Hennel F, Hennig J. Quiet imaging with interleaved spiral read-out. *Magn Reson Imaging*. 2001;19:1333-1337.
15. Schmitter S, Bock M. Acoustic noise-optimized VERSE pulses. *Magn Reson Med*. 2010;64:1447-1453.
16. Heismann B, Ott M, Grodzki D. Sequence-based acoustic noise reduction of clinical MRI scans. *Magn Reson Med*. 2015;73:1104-1109.
17. Versteeg E, Klomp DWJ, Siero JCW. A silent gradient axis for soundless spatial encoding to enable fast and quiet brain imaging. *Magn Reson Med*. 2022;87:1062-1073.
18. Brummett RE, Talbot JM, Charuhas P. Potential hearing loss resulting from MR imaging. *Radiology*. 1988;169:539-540.
19. International Electrotechnical Commission. Medical electrical equipment—part 2-33: particular requirements for the safety of magnetic resonance equipment for medical diagnosis. IEC 60601-2-33. 2022.
20. Counter SA, Olofsson A, Grahn H-F, Borg E. MRI acoustic noise: sound pressure and frequency analysis. *J Magn Reson Imaging*. 1997;7:606-611.
21. Hoffmann J, Henning A, Giapitzakis IA, et al. Safety testing and operational procedures for self-developed radiofrequency coils. *NMR Biomed*. 2016;29:1131-1144.
22. Lee BJ, Watkins RD, Chang C-M, Levin CS. Low Eddy current RF shielding enclosure designs for 3T MR applications. *Magn Reson Med*. 2018;79:1745-1752.
23. Weyers D, Liu Q. An RF shield comparative study of different materials and types. *In: Proc Intl Soc Magn Reson Med*. 2004; p. 1624.

SUPPORTING INFORMATION

Additional supporting information may be found in the online version of the article at the publisher's website.

Figure S1. Sound pressure levels in EPI for different readout axes and versus ES, with the reference RF shield and with the PBM shield but with no segmentation (no slits). Results are available for the right ear location only. The absence of slits in the PBM shield yielded higher sound pressure levels.

How to cite this article: Boulant N, Ma S, Walker E, et al. Acoustic noise reduction in the NexGen 7 T scanner. *Magn Reson Med*. 2024;1-10. doi: 10.1002/mrm.30211